View metadata, citation and similar papers at core.ac.uk
brought to you by CORE
provided by NASA Technical Reports Server

TN 1660

[redacted]

TECH LIBRARY KAFB, NM
0143111

939

NATIONAL ADVISORY COMMITTEE FOR AERONAUTICS

REPORT 939

THEORETICAL CHARACTERISTICS IN SUPERSONIC FLOW OF TWO TYPES OF CONTROL SURFACES ON TRIANGULAR WINGS

By WARREN A. TUCKER and ROBERT L. NELSON

1949

For sale by the Superintendent of Documents, U. S. Government Printing Office, Washington 25, D. C. Yearly subscription, $3.00; foreign, $4.50; single copy price varies according to size. - - - - - - - - - - Price 20 cents

AERONAUTIC SYMBOLS

1. FUNDAMENTAL AND DERIVED UNITS

	Symbol	Metric		English	
		Unit	Abbreviation	Unit	Abbreviation
Length	l	meter	m	foot (or mile)	ft (or mi)
Time	t	second	s	second (or hour)	sec (or hr)
Force	F	weight of 1 kilogram	kg	weight of 1 pound	lb
Power	P	horsepower (metric)		horsepower	hp
Speed	V	kilometers per hour meters per second	kph mps	miles per hour feet per second	mph fps

2. GENERAL SYMBOLS

W Weight $=mg$

g Standard acceleration of gravity $=9.80665$ m/s^2 or 32.1740 ft/sec^2

m Mass $=\frac{W}{g}$

I Moment of inertia $=mk^2$. (Indicate axis of radius of gyration k by proper subscript.)

μ Coefficient of viscosity

ν Kinematic viscosity

ρ Density (mass per unit volume)

Standard density of dry air, 0.12497 kg-m^{-4}-s^2 at 15° C and 760 mm; or 0.002378 lb-ft^{-4} sec^2

Specific weight of "standard" air, 1.2255 kg/m^3 or 0.07651 lb/cu ft

3. AERODYNAMIC SYMBOLS

S Area

S_w Area of wing

G Gap

b Span

c Chord

A Aspect ratio, $\frac{b^2}{S}$

V True air speed

q Dynamic pressure, $\frac{1}{2}\rho V^2$

L Lift, absolute coefficient $C_L=\frac{L}{qS}$

D Drag, absolute coefficient $C_D=\frac{D}{qS}$

D_0 Profile drag, absolute coefficient $C_{D_0}=\frac{D_0}{qS}$

D_i Induced drag, absolute coefficient $C_{D_i}=\frac{D_i}{qS}$

D_p Parasite drag, absolute coefficient $C_{D_p}=\frac{D_p}{qS}$

C Cross-wind force, absolute coefficient $C_C=\frac{C}{qS}$

i_w Angle of setting of wings (relative to thrust line)

i_t Angle of stabilizer setting (relative to thrust line)

Q Resultant moment

Ω Resultant angular velocity

R Reynolds number, $\rho\frac{Vl}{\mu}$ where l is a linear dimension (e.g., for an airfoil of 1.0 ft chord, 100 mph, standard pressure at 15° C, the corresponding Reynolds number is 935,400; or for an airfoil of 1.0 m chord, 100 mps, the corresponding Reynolds number is 6,865,000)

α Angle of attack

ϵ Angle of downwash

α_0 Angle of attack, infinite aspect ratio

α_i Angle of attack, induced

α_a Angle of attack, absolute (measured from zero-lift position)

γ Flight-path angle

TECH LIBRARY KAFB, NM
0143111

REPORT 939

THEORETICAL CHARACTERISTICS IN SUPERSONIC FLOW OF TWO TYPES OF CONTROL SURFACES ON TRIANGULAR WINGS

By WARREN A. TUCKER and ROBERT L. NELSON

Langley Aeronautical Laboratory
Langley Air Force Base, Va.

National Advisory Committee for Aeronautics

Headquarters, 1724 F Street NW., Washington 25, D. C.

Created by act of Congress approved March 3, 1915, for the supervision and direction of the scientific study of the problems of flight (U. S. Code, title 50, sec. 151). Its membership was increased from 12 to 15 by act approved March 2, 1929, and to 17 by act approved May 25, 1948. The members are appointed by the President, and serve as such without compensation.

JEROME C. HUNSAKER, Sc. D., Massachusetts Institute of Technology, *Chairman*

ALEXANDER WETMORE, Sc. D., Secretary, Smithsonian Institution, *Vice Chairman*

HON. JOHN R. ALISON, Assistant Secretary of Commerce.

DETLEV W. BRONK, PH. D., President, Johns Hopkins University.

KARL T. COMPTON, PH. D., Chairman, Research and Development Board, Department of Defense.

EDWARD U. CONDON, PH. D., Director, National Bureau of Standards.

JAMES H. DOOLITTLE, Sc. D., Vice President, Shell Union Oil Corp.

R. M. HAZEN, B. S., Director of Engineering, Allison Division, General Motors Corp.

WILLIAM LITTLEWOOD, M. E., Vice President, Engineering, American Airlines, Inc.

THEODORE C LONNQUEST, Rear Admiral, United States Navy, Deputy and Assistant Chief of the Bureau of Aeronautics.

DONALD L. PUTT, Major General, United States Air Force, Director of Research and Development, Office of the Chief of Staff, Matériel.

JOHN D. PRICE, Vice Admiral, United States Navy, Vice Chief of Naval Operations.

ARTHUR E. RAYMOND, Sc. D., Vice President, Engineering, Douglas Aircraft Co., Inc.

FRANCIS W. REICHELDERFER, Sc. D., Chief, United States Weather Bureau.

HON. DELOS W. RENTZEL, Administrator of Civil Aeronautics, Department of Commerce.

HOYT S. VANDENBERG, General, Chief of Staff, United States Air Force.

THEODORE P. WRIGHT, Sc. D., Vice President for Research, Cornell University.

HUGH L. DRYDEN, PH. D., *Director*

JOHN W. CROWLEY, JR., B. S., *Associate Director for Research*

JOHN F. VICTORY, LL. M., *Executive Secretary*

E. H. CHAMBERLIN, *Executive Officer*

HENRY J. REID, D. Eng., Director, Langley Aeronautical Laboratory, Langley Field, Va.

SMITH J. DEFRANCE, B. S., Director, Ames Aeronautical Laboratory, Moffett Field, Calif.

EDWARD R. SHARP, Sc. D., Director, Lewis Flight Propulsion Laboratory, Cleveland Airport, Cleveland, Ohio

TECHNICAL COMMITTEES

AERODYNAMICS
POWER PLANTS FOR AIRCRAFT
AIRCRAFT CONSTRUCTION
OPERATING PROBLEMS
INDUSTRY CONSULTING

Coordination of Research Needs of Military and Civil Aviation
Preparation of Research Programs
Allocation of Problems
Prevention of Duplication
Consideration of Inventions

LANGLEY AERONAUTICAL LABORATORY
Langley Field, Va.

LEWIS FLIGHT PROPULSION LABORATORY
Cleveland Airport, Cleveland, Ohio

AMES AERONAUTICAL LABORATORY
Moffett Field, Calif.

Conduct, under unified control, for all agencies of scientific research on the fundamental problems of flight

OFFICE OF AERONAUTICAL INTELLIGENCE
Washington, D. C.

Collection, classification, compilation, and dissemination of scientific and technical information on aeronautics

REPORT 939

THEORETICAL CHARACTERISTICS IN SUPERSONIC FLOW OF TWO TYPES OF CONTROL SURFACES ON TRIANGULAR WINGS

By Warren A. Tucker and Robert L. Nelson

SUMMARY

Methods based on the linearized theory for supersonic flow were used to find the characteristics of two types of control surfaces on thin triangular wings. The first type, the constant-chord partial-span flap, was considered to extend either outboard from the center of the wing or inboard from the wing tip. The second type, the full-triangular-tip flap, was treated only for the case in which the Mach number component normal to the leading edge is supersonic. For each type, expressions were found for the lift, rolling-moment, pitching-moment, and hinge-moment characteristics.

Calculations were made from the equations to illustrate various points of interest. A major conclusion was that flaps of the triangular-tip category are more suitable than constant-chord flaps for use as control surfaces on triangular wings, particularly when used as ailerons. Not only is the effectiveness of the triangular-tip flap in general greater than that of the constant-chord flap having the same area but the problem of providing hinge-moment balance is inherently simpler for the triangular-tip flap.

INTRODUCTION

There is a certain amount of interest in the use of wings having triangular plan forms for flight at supersonic speeds, and some work has been done on the aerodynamic characteristics of such wings (references 1 to 5). Investigation of the characteristics of control surfaces which might be used on triangular wings was therefore considered desirable.

A variety of control-surface arrangements has been suggested for use on triangular wings. Two such arrangements are the constant-chord partial-span flap (extending either outboard from the center of the wing or inboard from the tip of the wing) and the full-triangular-tip flap, which is located at the tip of the wing and has a plan form geometrically similar to that of the wing. (See fig. 1.) The analysis of these two types of control surface forms the subject of the present report. The full-triangular-tip flap is treated only for the case in which the Mach lines from the apex of the wing lie behind the leading edge (supersonic leading edge); the subsonic-leading-edge case is analyzed in reference 6, together with more general types of triangular-tip controls.

Methods based on the linearized equations for supersonic flow are used in the analysis, so the results are subject to the usual limitations of the linearized theory. Viscous effects have been neglected.

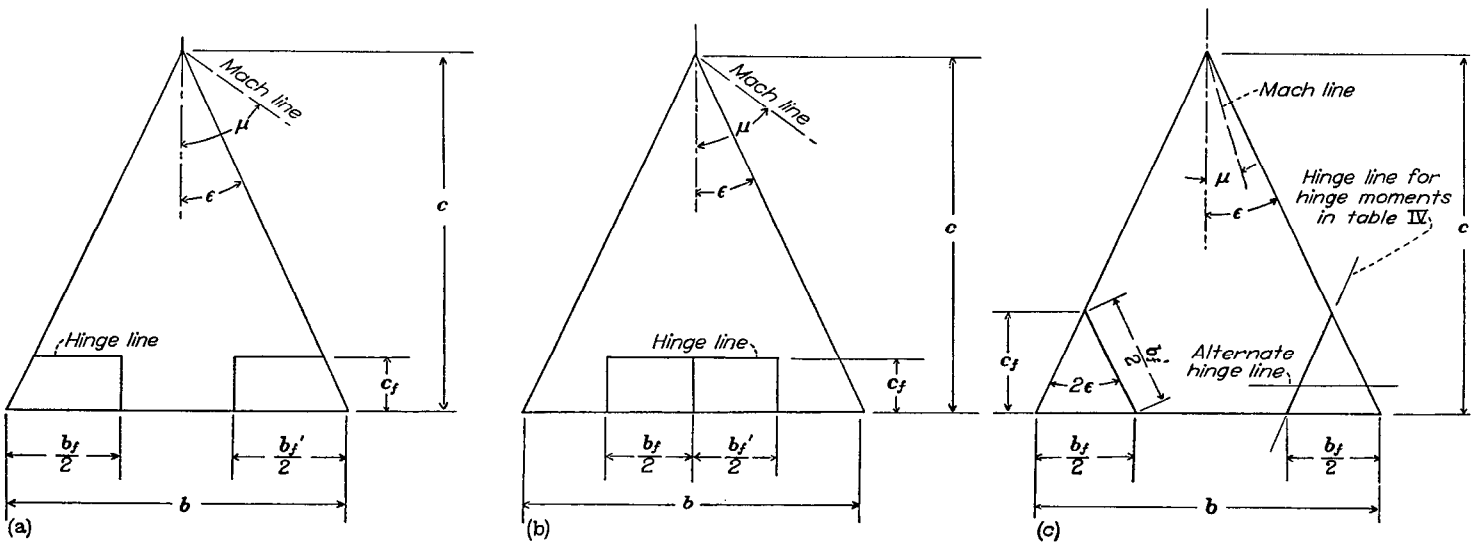

(a) Outboard constant-chord flaps.

(b) Inboard constant-chord flaps.

(c) Full-triangular-tip flaps.

FIGURE 1.—The control-surface configurations investigated.

SYMBOLS

b	maximum wing span
b_f	total maximum flap span normal to free stream
b_f'	total maximum flap span parallel to hinge line ($b_f'=b_f$ for constant-chord flap; see fig. 1)
c	wing root chord
c_l	wing local chord
$\bar{c}$	wing mean aerodynamic chord $\left(\frac{2}{S}\int_0^{b/2} c_l^2\,dy=\frac{2}{3}c\right)$
c_f	flap chord
$\bar{c}_f$	flap root-mean-square chord perpendicular to hinge line
C_L	Lift coefficient $\left(\frac{L}{qS}\right)$
C_m	pitching-moment coefficient about wing aerodynamic center $\left(\frac{M}{qS\bar{c}}\right)$
C_l	rolling-moment coefficient $\left(\frac{l}{qSb}\right)$
C_h	hinge-moment coefficient $\left(\frac{H}{qb_f'\bar{c}_f^2}\right)$
C_p	lifting pressure coefficient $\left(\frac{P}{q}\right)$
$E\left(\sqrt{1-m^2}\right)$	complete elliptic integral of second kind with modulus $\sqrt{1-m^2}$ (used in table I, equation (6))
H	hinge moment of two flaps
$k\equiv\cot\epsilon$	
L	lift of two flaps
l	rolling moment of two flaps, each deflected an amount δ in opposite directions
M	free-stream Mach number; pitching moment of two flaps about wing aerodynamic center $\left(\text{at } \frac{2}{3}c\right)$
$m\equiv\frac{\tan\epsilon}{\tan\mu}$	
P	lifting pressure
q	free-stream dynamic pressure $\left(\frac{\rho V^2}{2}\right)$
S	wing area
S_f	area of two flaps
$t\equiv\frac{y}{x\tan\epsilon}$	
V	free-stream velocity
w	vertical disturbance velocity (δV)
x, y	Cartesian coordinates parallel and normal, respectively, to free-stream direction (for field points)
ξ, η	Cartesian coordinates parallel and normal to free-stream direction (for source points)
α	angle of attack
$\beta\equiv\sqrt{M^2-1}$	
δ	angle of flap deflection in free-stream direction
ϵ	wing semiapex angle
$\zeta\equiv\tan^{-1}\frac{y}{x}$	
μ	Mach angle $\left(\tan^{-1}\frac{1}{\beta}\right)$
$\nu\equiv\frac{\beta y}{x}\equiv\frac{y/x}{\tan\mu}$	
ρ	free-stream density
ϕ	disturbance-velocity potential
ϕ_x	disturbance velocity in x-direction

Subscripts:

α	partial derivative of coefficient with respect to α $\left(\text{example: } C_{h_\alpha}\equiv\frac{\partial C_h}{\partial\alpha}\right)$
δ	partial derivative of coefficient with respect to δ
C_L	partial derivative of coefficient with respect to C_L
∞	infinite-span or two-dimensional wing condition

All angles are in radians, unless otherwise specified.

ANALYSIS

The two types of control surfaces (constant-chord flap and full-triangular-tip flap) are most conveniently considered separately. For each case the control-surface characteristics to be determined are as follows:

C_{L_δ}	lift coefficient due to flap deflection
C_{l_δ}	rolling-moment coefficient due to flap deflection
$C_{m_{C_L}}$	pitching-moment coefficient due to flap lift
C_{h_δ}	hinge-moment coefficient due to flap deflection
C_{h_α}	hinge-moment coefficient due to angle of attack

CONSTANT-CHORD PARTIAL-SPAN FLAP

Pressure distributions.—Any of the aforementioned control-surface characteristics can be found for the constant-chord partial-span flap if the pressure distributions due to flap deflection at constant angle of attack and due to angle of attack at constant flap deflection are known. This fact is true because of the principle of superposition.

The pressure distributions over certain regions of the flaps and over the wings are already known. For both the inboard flaps and the outboard flaps, the pressure due to flap deflection in the region between the Mach cones springing from the inner and outer corners of the flap is equal to the pressure on an infinite-span wing at an angle of attack. The pressure due to flap deflection in the tip Mach cone of the outboard flap when the Mach lines are ahead of the leading edge has been found from material in reference 7. The pressure distributions over the wing due to angle of attack have been found in reference 2 (Mach lines behind the leading edge) and reference 4 (Mach lines ahead of the leading edge).

There remain to be determined only the pressure distributions due to flap deflection in the following regions: First, the inner Mach cone of the outboard flap and the inner and outer Mach cones of the inboard flap (all three cases are identical); and, second, the tip of the outboard flap when the Mach lines are behind the leading edge. The pressure distribution for the first case is given in appendix A and for the second case, in appendix B.

The various pressure distributions are shown graphically in figures 2 and 3. The equations for the pressure distributions are as follows:

For figure 2 (a),

$$\frac{C_{p_1}}{\delta}=\frac{4}{\pi\beta}\cos^{-1}-\nu$$

$$\frac{C_{p_2}}{\delta}=\frac{4}{\beta}$$

$$\frac{C_{p_3}}{\delta}=\frac{4}{\pi\beta}\left[\cos^{-1}\nu+\frac{m}{\sqrt{m^2-1}}\cos^{-1}\left(\frac{1-m\nu}{m-\nu}\right)\right]$$

$$\frac{C_{p_4}}{\delta}=\frac{4m}{\beta\sqrt{m^2-1}}$$

For figure 2 (b),

$$\frac{C_{p_1}}{\delta}=\frac{4}{\pi\beta}\cos^{-1}-\nu$$

$$\frac{C_{p_2}}{\delta}=\frac{4}{\beta}$$

$$\frac{C_{p_3}}{\delta}=\frac{8}{\pi\beta}\left(\frac{m}{1\mp m}\sqrt{\frac{1\mp\nu}{m-\nu}}+\tan^{-1}\sqrt{\frac{m-\nu}{1\mp\nu}}\right)$$

For figure 2 (c),

$$\frac{C_{p_1}}{\delta}=\frac{4}{\pi\beta}\cos^{-1}-\nu$$

$$\frac{C_{p_2}}{\delta}=\frac{4}{\beta}$$

$$C_{p_3}=C_{p_1}$$

For figure 3 (a),

$$\frac{C_{p_1}}{\alpha}=\frac{C_{p_3}}{\alpha}=\frac{4m}{\beta\sqrt{m^2-1}}$$

$$\frac{C_{p_2}}{\alpha}=\frac{8m}{\pi\beta\sqrt{m^2-1}}\cos^{-1}\frac{1}{m}\sqrt{\frac{1-m^2t^2}{1-t^2}}$$

For figure 3 (b),

$$\frac{C_p}{\alpha}=\frac{4m}{\beta E(\sqrt{1-m^2})\sqrt{1-t^2}}$$

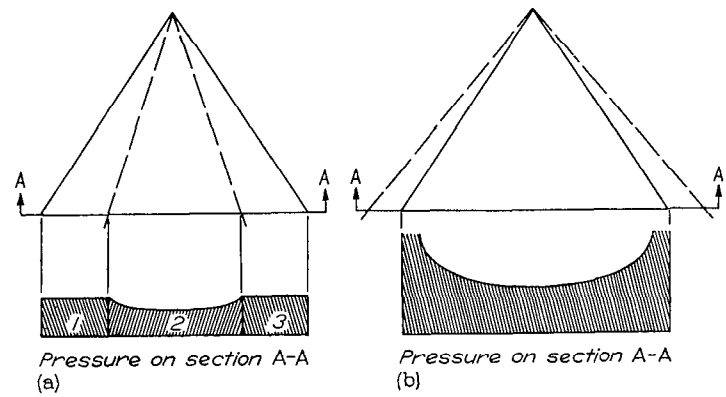

(a) $m \geqq 1$ (reference 2). (b) $m \leqq 1$ (reference 4).

FIGURE 3.—Pressure distributions due to angle of attack.

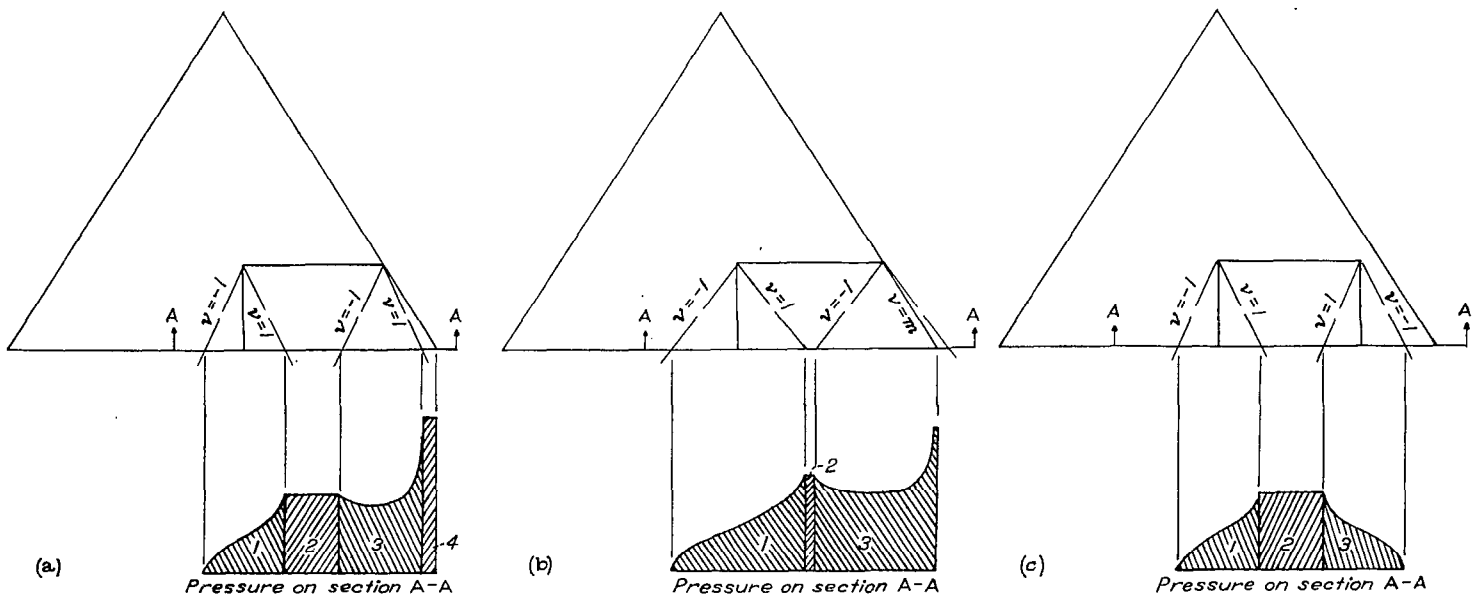

(a) Outboard flap; $m \geqq 1$. (b) Outboard flap; $m \leqq 1$. (c) Inboard flap.

FIGURE 2.—Pressure distributions due to flap deflection. Constant-chord flaps.

Derivation of control-surface characteristics.—Once the pressure distributions are known, the various control-surface characteristics can be found by integrating the pressure over the proper areas, multiplying by appropriate center-of-pressure distances when necessary, and dividing by the proper dimensions to form coefficients. Giving all the derivations for the cases treated in the present report would cause the report to be unduly lengthy; therefore, only one sample derivation is given.

The example chosen is C_{h_δ} for the outboard flap for the case in which the Mach lines are ahead of the leading edge. The equations for the pressure distribution are found from figure 2. Consider first the inner Mach cone. Integrating the pressure only over the part of the flap contained in the Mach cone (since the pressure on the wing contributes no hinge moment) gives for the lift on this part of the flap

$$\frac{L}{q\delta}=\frac{2c_f^2}{\beta^2}\left(\frac{\pi-1}{\pi}\right)$$

and, since the pressure distribution in the Mach cone is conical, the center of pressure of this lift is $\frac{2}{3}c_f$ behind the hinge line. The hinge moment on this part of the flap is then

$$\frac{H}{q\delta}=-\frac{2}{3}c_f\frac{2c_f^2}{\beta^2}\left(\frac{\pi-1}{\pi}\right)=-\frac{4}{3}\frac{c_f^3}{\beta^2}\left(\frac{\pi-1}{\pi}\right)$$

Next, for the part of the flap contained between the inner and outer Mach cones, the pressure over this entire region is noted to be constant at the two-dimensional value, so that the hinge moment can be found simply by multiplying the pressure by the moment of the trapezoidal area about the hinge line which gives

$$\frac{H}{q\delta}=\frac{6m+8}{3}\frac{c_f^3}{\beta^2}-b_f\frac{c_f^2}{\beta}$$

The lift in the tip region has been found from integration of the pressure distribution to be

$$\frac{L}{q\delta}=\frac{c_f^2}{\beta^2}(3m+1)$$

and, since the flow in the tip region is conical, the hinge moment is

$$\frac{H}{q\delta}=-\frac{2}{3}c_f\frac{c_f^2}{\beta^2}(3m+1)=-\frac{2}{3}\frac{c_f^3}{\beta^2}(3m+1)$$

Adding the three hinge moments gives the total hinge moment

$$\frac{H}{q\delta}=-b_f\frac{c_f^2}{\beta}+\frac{2\pi+4}{3\pi}\frac{c_f^3}{\beta^2}$$

The hinge-moment coefficient is formed by dividing the total hinge moment by $b_f\bar{c}_f^2/2$, which in this case is found to be

$$\frac{b_f\bar{c}_f^2}{2}=\frac{b_fc_f^2}{2}-\frac{2}{3}m\frac{c_f^3}{\beta}$$

Performing the division yields

$$C_{h_\delta}\frac{\beta}{2}=-\frac{3\frac{b_f}{b}-\frac{1}{m}\frac{\pi+2}{\pi}\frac{c_f}{c}}{3\frac{b_f}{b}-2\frac{c_f}{c}}$$

The other control-surface characteristics may be derived in a similar manner. Before giving the final equations, however, a short discussion of the range of applicability is advisable.

Range of applicability.—Both in the discussion of pressure distributions and in the sample derivation of one of the control-surface characteristics, the Mach lines were tacitly assumed to have had the positions shown in figure 2. Many other cases are possible; for example, two Mach lines may intersect or a Mach line from one corner of a flap may cross the leading edge of the wing. These various cases have been examined to determine over just what range each equation is applicable. The method used to determine the range of applicability is given in appendix C. The limits are conveniently expressed as the minimum and maximum values of b_f/b that can be used for given values of c_f/c and m; it is in this form that the limits are given in tables I to IV.

FULL-TRIANGULAR-TIP FLAP

The analysis of the full-triangular-tip flap is for the most part very simple for the case in which the wing leading edge is supersonic ($m>1$) because there is no change in pressure over the main surface of the wing when the flap is deflected. Each flap can therefore be regarded as an isolated triangular wing so that the lift and center of pressure are known from reference 2. The problem of finding the derivatives C_{L_δ}, C_{l_δ}, $C_{m_{C_L}}$, and C_{h_δ} is then mainly one of simple algebra.

This simple concept cannot be used to determine the derivative C_{h_α}. Instead, a suitable integration of the pressure distribution of figure 3 (a) must be performed over the surface of the flap in much the same manner as for the constant-chord flap.

The range of applicability of the resulting equations for the characteristics of the full-triangular-tip flap is limited only by the conditions that the wing leading edge must be supersonic ($m>1$) and that the two flaps must not be so large as to interfere physically with each other $\left(\frac{c_f}{c}\leqq 0.5\right)$.

Although in calculating hinge moments the flap hinge line has been assumed to lie along the inboard edge of the flap, as shown in figure 1, it could equally well be in the alternate position shown. (The distance between the hinge line and the trailing edge is arbitrary.) Under the assumptions of the present theory, the only derivatives affected by the change would be the hinge-moment derivatives C_{h_δ} and C_{h_α}.

RESULTS AND DISCUSSION

The resulting equations for the control-surface characteristics are presented in tables I to IV, together with the range of applicability of each equation.

A comparison of inboard and outboard constant-chord flaps is afforded by figure 4, in which some of the control-surface characteristics are shown for a ratio of flap area to wing area of 0.2 and a value of $m=0.8$. As would be expected, the characteristics of the two types of flaps tend to become identical as the ratio of flap span to wing span approaches unity. Another point to notice is that small-chord large-span flaps are the most efficient when the lift per unit hinge moment $(-cL/H)$ is used as a criterion. This finding is consistent with subsonic experience with plain flaps.

The curve of $C_{l_\delta}\beta$ for outboard flaps in figure 4 shows the interesting fact that for a given flap-area ratio an optimum flap-span ratio exists which gives the greatest rolling-moment effectiveness. This optimum flap-span ratio has been found by differentiation of equations (2) and (8) (tables I and II) and is shown in figure 5 for various values of m. For $m>1$ (supersonic leading edge) the resultant flap is a half-triangular-tip control rotating about an axis normal to the stream, as shown by the small sketch in figure 5. The results shown in figure 5 are strictly applicable only to wings having zero thickness. The effect of finite thickness is discussed in the following paragraphs.

The half-triangular-tip flap and the constant-chord full-span flap can both be regarded as limiting cases of the constant-chord partial-span flap. The half-triangular-tip flap can also be thought of as belonging to the family of which the full-triangular-tip flap is a member. A comparison of the characteristics of the three flaps is therefore of interest. Such a comparison is given in figure 6 for a particular wing and ratio of flap area to wing area. The information necessary to obtain results for the triangular-tip flaps at Mach numbers less than $\sqrt{2}$ was taken from reference 6.

The curves of figures 5 and 6, having been obtained by the use of linearized theory, are strictly applicable only to wings of zero thickness. When wings having finite thickness are considered, the picture will change considerably. The effect of thickness will be to decrease the effectiveness of the constant-chord flaps; this effect is discussed in references 8 and 9. However, the streamwise sections of the triangular-tip flaps for the most part appear more as complete airfoil sections than as sections of trailing-edge flaps. The effect of finite thickness on the lift of a complete airfoil section is very small, so it is to be expected that the effectiveness of the triangular-tip flaps would change very little when finite thickness is considered. There are some experimental data which support these statements. When the curves of figure 6 are viewed with these considerations in mind, the conclusion is reached that triangular-tip flaps are more effective as controls on triangular wings than are constant-chord flaps, particularly so far as rolling moments are concerned.

No hinge moments are shown in figure 6 for the reason that they depend on the location of the hinge line. For either of the triangular-tip flaps the value of C_{h_δ} theoretically

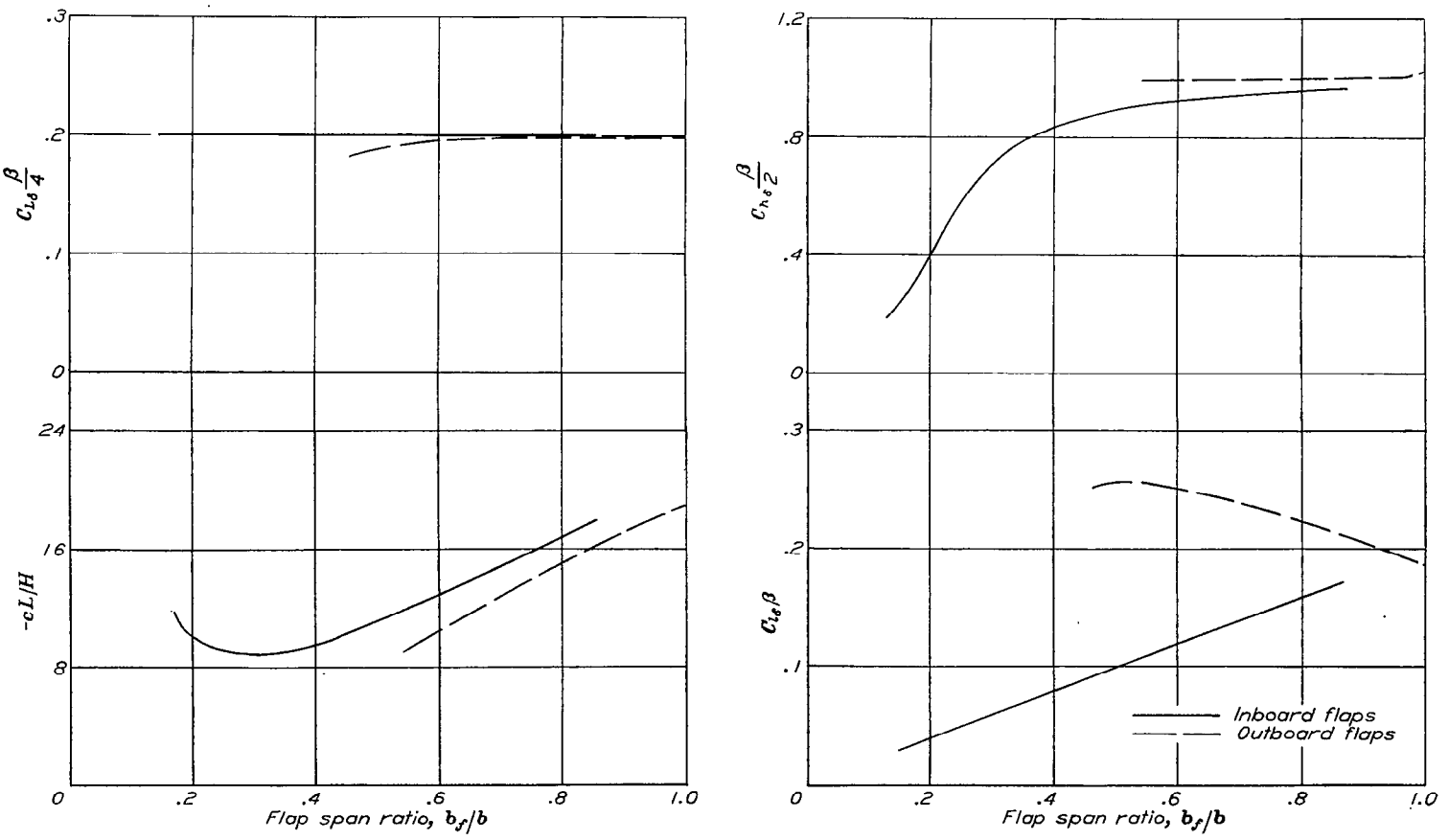

FIGURE 4.—Comparison of control-surface characteristics of inboard and outboard constant-chord flaps. $\frac{S_f}{S}=0.2$; $m=0.8$.

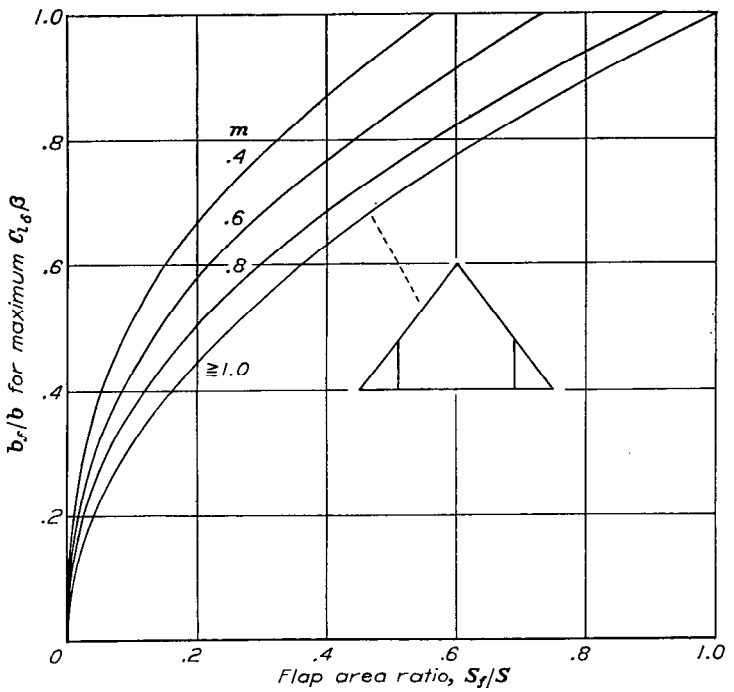

FIGURE 5.—Flap span ratio required for maximum rolling-moment effectiveness. Outboard constant-chord flaps.

will be zero at all supersonic Mach numbers if the hinge line passes through the center of area of the flap and is parallel to the trailing edge. In a practical case, the chordwise location of the center of pressure of the load due to flap deflection will probably not be at the center of area, and it will also probably shift some slight amount with Mach number. However, the problem of hinge-moment balance will certainly be less serious for triangular-tip flaps than for other types.

CONCLUDING REMARKS

The control-surface characteristics of constant-chord flaps and triangular-tip flaps on triangular wings were found by the use of methods based on the linearized theory for supersonic flow. Because of their generally higher effectiveness

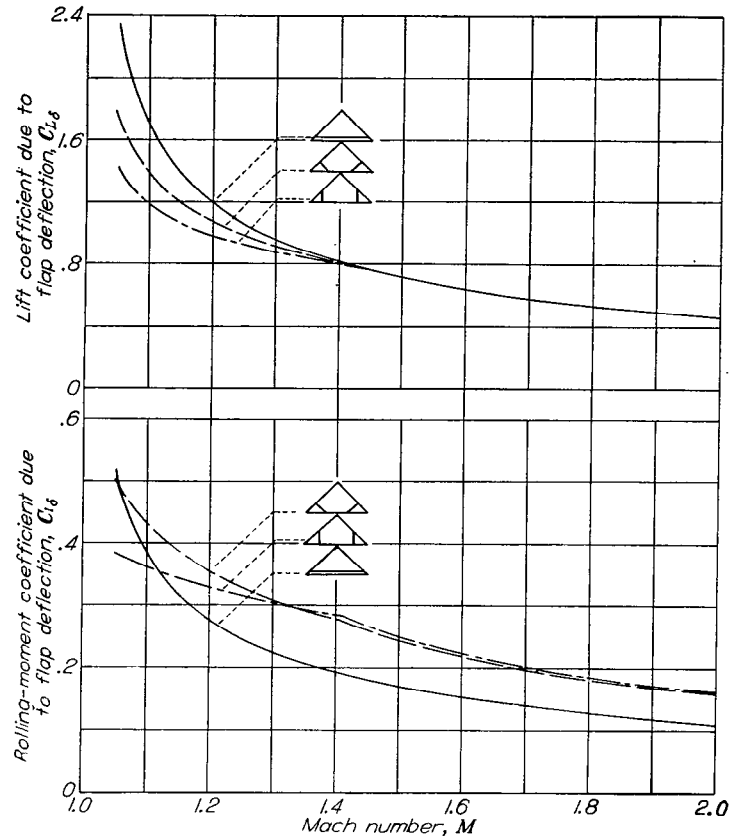

FIGURE 6.—Comparison of the characteristics of three types of control surfaces on a triangular wing. $\frac{S_f}{S}=0.2$; $\epsilon=45°$.

and less serious hinge-moment problems, triangular-tip flaps were concluded to be more satisfactory than constant-chord flaps for this application.

LANGLEY AERONAUTICAL LABORATORY,
NATIONAL ADVISORY COMMITTEE FOR AERONAUTICS,
LANGLEY AIR FORCE BASE, VA., *July 21, 1949.*

APPENDIX A

PRESSURE DISTRIBUTION OVER INBOARD CORNER OF FLAP

The flap in figure 7 may be represented by a uniform distribution of sources and sinks. If the chordwise gap between wing and flap is considered sealed, the pressure distribution due to flap deflection may be determined by the method of reference 2.

The equation for the surface velocity potential at a point (x,y) due to a uniform source distribution is given by reference 2 as

$$\phi(x,y)=-\frac{1}{\pi}\int\int\frac{w\ d\xi\ d\eta}{\sqrt{(x-\xi)^2-\beta^2(y-\eta)^2}}$$

where w is the vertical velocity and the area of integration is over the fore-cone of (x,y). Thus,

$$\phi(x,y)=-\frac{w}{\pi}\int_0^{y_1}d\eta\int_0^{x-\beta(\eta-y)}\frac{d\xi}{\sqrt{(x-\xi)^2-\beta^2(y-\eta)^2}}$$

The first integration (reference 10, equation 260.01) gives

$$\phi(x,y)=-\frac{w}{\pi}\int_0^{y_1}d\eta\left[-\cosh^{-1}\left|\frac{x-\xi}{\beta(y-\eta)}\right|\right]_0^{x-\beta(\eta-y)}$$

$$=-\frac{w}{\pi}\int_0^{y_1}\cosh^{-1}\frac{x}{\beta|\eta-y|}d\eta$$

Differentiation under the integral sign with respect to x results in

$$\phi_x(x,y)=-\frac{w}{\pi}\int_0^{y_1}\frac{d\eta}{\sqrt{x^2-\beta^2(\eta-y)^2}}$$

$$=-\frac{w}{\pi}\int_0^{y_1}\frac{d\eta}{\sqrt{x^2-\beta^2y^2+2\beta^2y\eta-\beta^2\eta^2}}$$

This integral can be evaluated (reference 10, equation 380.001) to give

$$\phi_x(x,y)=-\frac{w}{\pi}\left[-\frac{1}{\beta}\sin^{-1}\frac{\beta y-\beta\eta}{x}\right]_0^{y_1}$$

where at y_1

$$\eta=\frac{x+\beta y}{\beta}$$

Thus,

$$\phi_x(x,y)=-\frac{w}{\pi\beta}\left[-\sin^{-1}\frac{\beta y-(x+\beta y)}{x}+\sin^{-1}\frac{\beta y}{x}\right]$$

$$=-\frac{w}{\pi\beta}\left(\frac{\pi}{2}+\sin^{-1}\frac{\beta y}{x}\right)$$

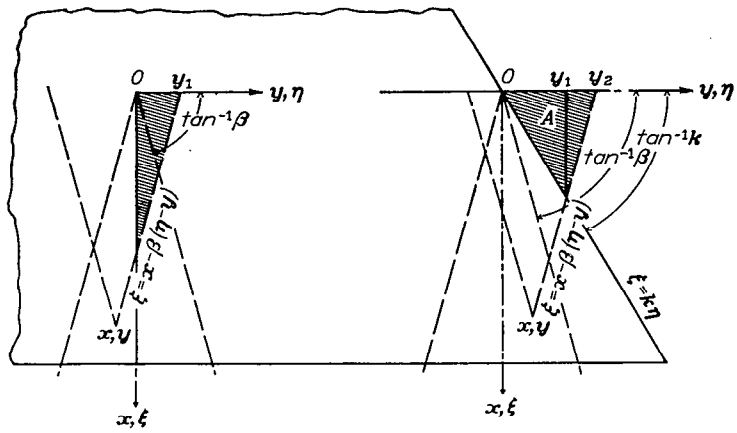

FIGURE 7.—Notation used in appendixes A and B.

Since ϕ_x is constant along lines $\frac{y}{x}$=constant, a new variable $\nu=\frac{\beta y}{x}$ is introduced.

Then,

$$\phi_x(x,y)=-\frac{w}{\pi\beta}\left(\frac{\pi}{2}+\sin^{-1}\nu\right)$$

or

$$\phi_x(x,y)=-\frac{w}{\pi\beta}\cos^{-1}(-\nu)$$

From reference 2 (taking into account upper and lower surfaces),

$$C_p=-\frac{4\phi_x}{V}$$

$$=\frac{4}{\pi\beta}\frac{w}{V}\left(\frac{\pi}{2}+\sin^{-1}\nu\right)$$

Since $\frac{w}{V}=\delta$,

$$C_p=\frac{4\delta}{\pi\beta}\left(\frac{\pi}{2}+\sin^{-1}\nu\right)$$

$$=\frac{4\delta}{\pi\beta}\cos^{-1}(-\nu)$$

865171—50——2

APPENDIX B

PRESSURE ON OUTER CORNER OF OUTBOARD FLAPS ($m>1$)

The pressure within the Mach cone over the outboard corner of the flap when the Mach line lies behind the leading edge of the flap (see fig. 7) may be determined in a manner similar to that of appendix A. The equation for the potential is then the two-dimensional value $-\frac{wx}{\beta}$ minus the contribution from the source distribution in area A. Then,

$$\phi(x,y)=-\frac{wx}{\beta}+\frac{w}{\pi}\int_0^{y_1}d\eta\int_0^{k\eta}\frac{d\xi}{\sqrt{(x-\xi)^2-\beta^2(y-\eta)^2}}+$$
$$\frac{w}{\pi}\int_{y_1}^{y_2}d\eta\int_0^{x-\beta(\eta-y)}\frac{d\xi}{\sqrt{(x-\xi)^2-\beta^2(y-\eta)^2}}$$

The first integration (reference 10, equation 260.01) gives

$$\phi(x,y)=-\frac{wx}{\beta}+\frac{w}{\pi}\int_0^{y_1}d\eta\left[-\cosh^{-1}\left|\frac{x-\xi}{\beta(y-\eta)}\right|\right]_0^{k\eta}+$$
$$\frac{w}{\pi}\int_{y_1}^{y_2}d\eta\left[-\cosh^{-1}\left|\frac{x-\xi}{\beta(y-\eta)}\right|\right]_0^{x-\beta(\eta-y)}$$
$$=-\frac{wx}{\beta}+\frac{w}{\pi}\int_0^{y_1}\cosh^{-1}\left|\frac{x}{\beta(y-\eta)}\right|d\eta-$$
$$\frac{w}{\pi}\int_0^{y_1}\cosh^{-1}\left|\frac{x-k\eta}{\beta(y-\eta)}\right|d\eta+\frac{w}{\pi}\int_{y_1}^{y_2}\cosh^{-1}\left|\frac{x}{\beta(y-\eta)}\right|d\eta$$
$$=-\frac{wx}{\beta}+\frac{w}{\pi}\int_0^{y_2}\cosh^{-1}\left|\frac{x}{\beta(y-\eta)}\right|d\eta-$$
$$\frac{w}{\pi}\int_0^{y_1}\cosh^{-1}\left|\frac{x-k\eta}{\beta(y-\eta)}\right|d\eta$$

Differentiation with respect to x to obtain ϕ_x gives

$$\phi_x(x,y)=-\frac{w}{\beta}+\frac{w}{\pi}\int_0^{y_2}\frac{d\eta}{\sqrt{x^2-\beta^2(y-\eta)^2}}-\frac{w}{\pi}\int_0^{y_1}\frac{d\eta}{\sqrt{(x-k\eta)^2-\beta^2(y-\eta)^2}}$$
$$=-\frac{w}{\beta}+\frac{w}{\pi}\int_0^{y_2}\frac{d\eta}{\sqrt{x^2-\beta^2y^2+2\beta^2y\eta-\beta^2\eta^2}}-$$
$$\frac{w}{\pi}\int_0^{y_1}\frac{d\eta}{\sqrt{x^2-\beta^2y^2+2(\beta^2y-kx)\eta-(\beta^2-k^2)\eta^2}}$$

The integrals can be evaluated (reference 10, equation 380.001) to give

$$\phi_x(x,y)=-\frac{w}{\beta}+\frac{w}{\pi}\left[-\frac{1}{\beta}\sin^{-1}\frac{\beta y-\beta\eta}{x}\right]_0^{x+\beta y}-$$
$$\frac{w}{\pi}\left[-\frac{1}{\sqrt{\beta^2-k^2}}\sin^{-1}\frac{\beta^2y-kx-(\beta^2-k^2)\eta}{\beta(x-ky)}\right]_0^{\frac{x+\beta y}{\beta+k}}$$
$$=-\frac{w}{\beta}+\frac{w}{\pi\beta}\left(\frac{\pi}{2}+\sin^{-1}\frac{\beta y}{x}\right)-$$
$$\frac{w}{\pi\sqrt{\beta^2-k^2}}\left[\frac{\pi}{2}-\sin^{-1}\frac{kx-\beta^2y}{\beta(x-ky)}\right]$$
$$=-\frac{w}{\pi\beta}\left(\pi-\frac{\pi}{2}-\sin^{-1}\frac{\beta y}{x}\right)-$$
$$\frac{w}{\pi\sqrt{\beta^2-k^2}}\cos^{-1}\frac{kx-\beta^2y}{\beta(x-ky)}$$
$$=-\frac{w}{\pi\beta}\cos^{-1}\frac{\beta y}{x}-\frac{w}{\pi\beta\sqrt{1-\frac{k^2}{\beta^2}}}\cos^{-1}\frac{k\left(1-\frac{\beta^2y}{kx}\right)}{\beta\left(1-\frac{k\beta y}{\beta x}\right)}$$

Let $\nu=\frac{\beta y}{x}$ and $m=\frac{\beta}{k}$; then,

$$\phi_x(x,y)=-\frac{w}{\pi\beta}\left[\cos^{-1}\nu+\frac{m}{\sqrt{m^2-1}}\cos^{-1}\left(\frac{1-m\nu}{m-\nu}\right)\right]$$

Since $C_p=-\frac{4\phi_x}{V}$ and $w=\delta V$,

$$C_p=\frac{4\delta}{\pi\beta}\left[\cos^{-1}\nu+\frac{m}{\sqrt{m^2-1}}\cos^{-1}\left(\frac{1-m\nu}{m-\nu}\right)\right]$$

When $\nu=1$, this expression for C_p becomes

$$C_p=\frac{4m}{\beta\sqrt{m^2-1}}$$

The pressure is constant at this value everywhere outboard of the Mach cone.

APPENDIX C

METHOD OF DETERMINING THE RANGE OF APPLICABILITY

As an illustrative example, consider an outboard flap with the Mach lines ahead of the leading edge and suppose that two Mach lines cross on the flap. (See fig. 8.) It is to be determined if the equation for the lift due to flap deflection (to take a simple example) is the same equation that would be obtained if the Mach lines did not cross. The test may be made in the following manner.

First, determine the pressure coefficients in the various areas indicated by numbers in figure 8. In region 1

$$C_{p_1}=C_{p_\infty}$$

$$C_{p_2}=C_{p_\infty}-\Delta C_{p_2}$$

where ΔC_{p_2} is the result of the inboard tip effect so that

$$\Delta C_{p_2}=C_{p_\infty}-C_{p_2}$$

Similarly,

$$C_{p_3}=C_{p_\infty}-\Delta C_{p_3}$$

where ΔC_{p_3} is the result of the outboard tip effect so that

$$\Delta C_{p_3}=C_{p_\infty}-C_{p_3}$$

Now,

$$C_{p_4}=C_{p_\infty}-\Delta C_{p_2}-\Delta C_{p_3}$$

or

$$C_{p_4}=C_{p_2}+C_{p_3}-C_{p_\infty}$$

The lift per unit flap deflection is

$$\begin{aligned}\frac{L}{q\delta}&=\frac{1}{\delta}\left(\int_{S_1}C_{p_1}dS+\int_{S_2}C_{p_2}dS+\int_{S_3}C_{p_3}dS+\int_{S_4}C_{p_4}dS\right)\\&=\frac{1}{\delta}\left(\int_{S_1}C_{p_\infty}dS+\int_{S_2}C_{p_2}dS+\int_{S_3}C_{p_3}dS+\int_{S_4}C_{p_2}dS+\int_{S_4}C_{p_3}dS-\int_{S_4}C_{p_\infty}dS\right)\\&=\frac{1}{\delta}\left(\int_{S_1-S_4}C_{p_\infty}dS+\int_{S_2+S_4}C_{p_2}dS+\int_{S_3+S_4}C_{p_3}dS\right)\end{aligned}$$

Now, if the total area affected is written as

$$S_f'=S_1+S_2+S_3+S_4$$

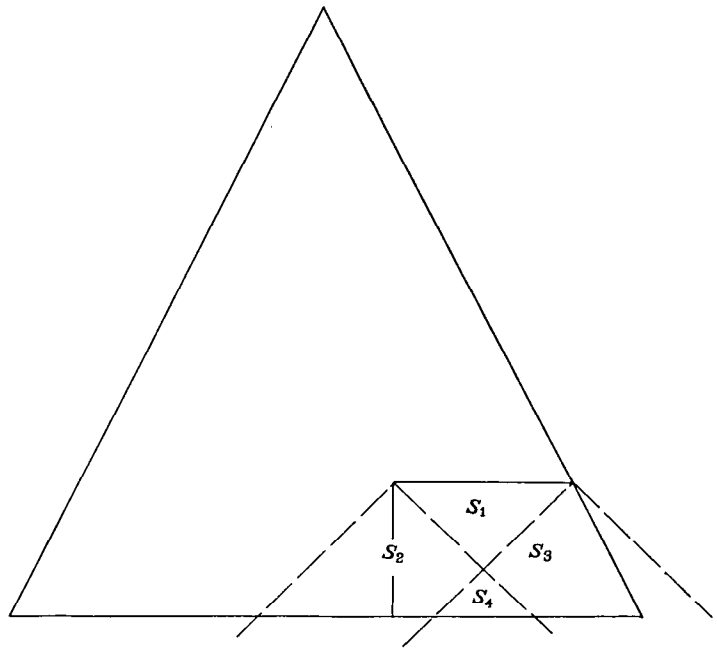

FIGURE 8.—Notation used in appendix C.

then

$$S_1-S_4=S_f'-(S_2+S_4)-(S_3+S_4)$$

The area covered by the inner Mach cone is S_2+S_4 and the area covered by the outer Mach cone is S_3+S_4, so that the final equation for $L/q\delta$ can be written as

$$\frac{L}{q\delta}=\frac{1}{\delta}\,[C_{p_\infty}\,(\text{Total area affected}-\text{Area in inner Mach cone}-\text{Area in outer Mach cone})+\text{Lift in inner Mach cone}+\text{Lift in outer Mach cone}]$$

which is exactly the same equation that is used when the Mach lines do not cross.

This method is very convenient to use, since no lengthy integrations need be performed. Although a lift case was used as an example, the extension to other cases (hinge moment, rolling moment, and so forth) is not difficult.

REFERENCES

1. Brown, Clinton E.: Theoretical Lift and Drag of Thin Triangular Wings at Supersonic Speeds. NACA Rep. 839, 1946.
2. Puckett, Allen E.: Supersonic Wave Drag of Thin Airfoils. Jour. Aero. Sci., vol. 13, no. 9, Sept. 1946, pp. 475–484.
3. Brown, Clinton E., and Adams, Mac C.: Damping in Pitch and Roll of Triangular Wings at Supersonic Speeds. NACA Rep. 892, 1948.
4. Stewart, H. J.: The Lift of a Delta Wing at Supersonic Speeds. Quarterly Appl. Math., vol. IV, no. 3, Oct. 1946, pp. 246–254.
5. Ribner, Herbert S., and Malvestuto, Frank S., Jr.: Stability Derivatives of Triangular Wings at Supersonic Speeds. NACA Rep. 908, 1948.
6. Lagerstrom, P. A., and Graham, Martha E.: Linearized Theory of Supersonic Control Surfaces. Jour. Aero. Sci., vol. 16, no. 1, Jan. 1949, pp. 31–34.
7. Evvard, John C.: Distribution of Wave Drag and Lift in the Vicinity of Wing Tips at Supersonic Speeds. NACA TN 1382, 1947.
8. Ivey, H. Reese: Notes on the Theoretical Characteristics of Two-Dimensional Supersonic Airfoils. NACA TN 1179, 1947.
9. Tucker, Warren A., and Nelson, Robert L.: Theoretical Characteristics in Supersonic Flow of Constant-Chord Partial-Span Control Surfaces on Rectangular Wings Having Finite Thickness. NACA TN 1708, 1948.
10. Dwight, Herbert Bristol: Tables of Integrals and Other Mathematical Data. Rev. ed., The Macmillan Co., 1947.

TABLE I.—CHARACTERISTICS OF OUTBOARD FLAPS ON TRIANGULAR WINGS

[$m<1$, Mach lines ahead of leading edge]

Quantity	Equation number	Equation	Range	
			$(b_f/b)_{min}$	$(b_f/b)_{max}$
C_{L_δ}	1	$C_{L_\delta}=\frac{4}{\beta}\left[2\frac{b_f}{b}\frac{c_f}{c}-\frac{1+m}{2m}\left(\frac{c_f}{c}\right)^2\right]$	$\frac{1}{m}\frac{c_f}{c}$	1.0
C_{l_δ}	2	$C_{l_\delta}=\frac{2}{\beta}\left\{\left[2\frac{b_f}{b}-\left(\frac{b_f}{b}\right)^2\right]\frac{c_f}{c}-\frac{1+m}{2m}\left(\frac{c_f}{c}\right)^2+\frac{3m^2+6m-1}{24m^2}\left(\frac{c_f}{c}\right)^3\right\}$	$\frac{1}{m}\frac{c_f}{c}$	1.0
$C_{m_{C_L}}$	3	$C_{m_{C_L}}=-\frac{1}{2}\frac{4m\frac{b_f}{b}-\left[1+\left(1+6\frac{b_f}{b}\right)m\right]\frac{c_f}{c}+(1+3m)\left(\frac{c_f}{c}\right)^2}{4m\frac{b_f}{b}-(1+m)\frac{c_f}{c}}$	$\frac{1}{m}\frac{c_f}{c}$	1.0
C_{h_δ}	4	$C_{h_\delta}=-\frac{2}{\beta}\frac{3\frac{b_f}{b}-\frac{1}{m}\frac{\pi+2}{\pi}\frac{c_f}{c}}{3\frac{b_f}{b}-2\frac{c_f}{c}}$	$\left(1+\frac{1}{m}\right)\frac{c_f}{c}$	$1-\frac{1}{2m}\frac{c_f}{c}$
C_{h_δ}	5	$C_{h_\delta}=-\frac{2}{\beta}\frac{3\frac{b_f}{b}-\frac{1}{m}\frac{\pi+2}{\pi}\frac{c_f}{c}+\left[\frac{2}{m\pi}\frac{c_f}{c}+\frac{4m}{\pi}\frac{\left(1-\frac{b_f}{b}\right)^2}{c_f/c}\right]\sqrt{1-\frac{4m^2\left(1-\frac{b_f}{b}\right)^2}{(c_f/c)^2}}-\frac{6}{\pi}\left(1-\frac{b_f}{b}\right)\cos^{-1}\frac{2m\left(1-\frac{b_f}{b}\right)}{c_f/c}}{3\frac{b_f}{b}-2\frac{c_f}{c}}$	$\left(1+\frac{1}{m}\right)\frac{c_f}{c};\frac{c_f}{c}>\frac{2m}{1+2m}$ $\left(1-\frac{1}{2m}\right)\frac{c_f}{c};\frac{c_f}{c}<\frac{2m}{1+2m}$	1.0
C_{h_α}	6	$C_{h_\alpha}=-\frac{2}{\beta}\frac{m}{E(\sqrt{1-m^2})}\frac{1}{\left[3\frac{b_f}{b}\left(\frac{c_f}{c}\right)^2-2\left(\frac{c_f}{c}\right)^3\right]}\left\{\left(1-\frac{c_f}{c}\right)^3\cos^{-1}\frac{1-\frac{b_f}{b}}{1-\frac{c_f}{c}}-\left(1-3\frac{c_f}{c}\right)\cos^{-1}\left(1-\frac{b_f}{b}\right)-\left(1-\frac{b_f}{b}\right)^3\left[\cosh^{-1}\left(\frac{1}{1-\frac{b_f}{b}}\right)-\cosh^{-1}\left(\frac{1-\frac{c_f}{c}}{1-\frac{b_f}{b}}\right)\right]+\left(2-3\frac{c_f}{c}\right)\left(1-\frac{b_f}{b}\right)\sqrt{1-\left(1-\frac{b_f}{b}\right)^2}-2\left(1-\frac{c_f}{c}\right)\left(1-\frac{b_f}{b}\right)\sqrt{\left(1-\frac{c_f}{c}\right)^2-\left(1-\frac{b_f}{b}\right)^2}\right\}$	c_f/c	1.0

TABLE II.—CHARACTERISTICS OF OUTBOARD FLAPS ON TRIANGULAR WINGS

[$m>1$, Mach lines behind leading edge]

Quantity	Equation Number	Equation	Range	
			$(b_f/b)_{min}$	$(b_f/b)_{max}$
C_{L_δ}	7	$C_{L_\delta}=\frac{4}{\beta}\left[2\frac{b_f}{b}\frac{c_f}{c}-\left(\frac{c_f}{c}\right)^2\right]$	c_f/c	1.0
C_{l_δ}	8	$C_{l_\delta}=\frac{2}{\beta}\left\{\left[2\frac{b_f}{b}-\left(\frac{b_f}{b}\right)^2\right]\frac{c_f}{c}-\left(\frac{c_f}{c}\right)^2+\frac{1}{3}\left(\frac{c_f}{c}\right)^3\right\}$	c_f/c	1.0
$C_{m_{C_L}}$	9	$C_{m_{C_L}}=-\frac{2\frac{b_f}{b}-\left(1+3\frac{b_f}{b}\right)\frac{c_f}{c}+2\left(\frac{c_f}{c}\right)^2}{4\frac{b_f}{b}-2\frac{c_f}{c}}$	c_f/c	1.0
C_{h_δ}	10	$C_{h_\delta}=-\frac{2}{\beta}\frac{3\frac{b_f}{b}-\frac{1}{m}\frac{m\pi+2}{\pi}\frac{c_f}{c}}{3\frac{b_f}{b}-2\frac{c_f}{c}}$	$\left(1+\frac{1}{m}\right)\frac{c_f}{c}$	$1-\frac{1}{2m}\frac{c_f}{c}$
C_{h_δ}	11	$C_{h_\delta}=-\frac{2}{\beta}\frac{3\frac{b_f}{b}-\frac{1}{m}\frac{m\pi+2}{\pi}\frac{c_f}{c}+\left[\frac{2}{m\pi}\frac{c_f}{c}+\frac{4m}{\pi}\frac{\left(1-\frac{b_f}{b}\right)^2}{c_f/c}\right]\sqrt{1-\frac{4m^2\left(1-\frac{b_f}{b}\right)^2}{(c_f/c)^2}}-\frac{6}{\pi}\left(1-\frac{b_f}{b}\right)\cos^{-1}\frac{2m\left(1-\frac{b_f}{b}\right)}{c_f/c}}{3\frac{b_f}{b}-2\frac{c_f}{c}}$	$\left(1+\frac{1}{m}\right)\frac{c_f}{c};\ \frac{c_f}{c}>\frac{2m}{2m+1}$ $1-\frac{1}{2m}\frac{c_f}{c};\ \frac{c_f}{c}<\frac{2m}{2m+1}$	1.0
C_{h_α}	12	$C_{h_\alpha}=-\frac{2}{\beta}\frac{m}{\sqrt{m^2-1}}\frac{3\frac{b_f}{b}-\frac{c_f}{c}}{3\frac{b_f}{b}-2\frac{c_f}{c}}$	c_f/c	$\frac{m-1}{m}$
C_{h_α}	13	$C_{h_\alpha}=-\frac{2}{\beta}\frac{2}{\pi\beta\left[3\frac{b_f}{b}\left(\frac{c_f}{c}\right)^2-2\left(\frac{c_f}{c}\right)^3\right]}\left[\left(3\frac{c_f}{c}-1\right)\cos^{-1}\left[m\left(1-\frac{b_f}{b}\right)\right]-m\left(1-\frac{b_f}{b}\right)^3\cosh^{-1}\frac{1}{m\left(1-\frac{b_f}{b}\right)}+\frac{m}{\sqrt{m^2-1}}\left(\frac{\pi}{2}\left\{\left(\frac{c_f}{c}\right)^2\left(3-\frac{c_f}{c}\right)-\left(1-\frac{b_f}{b}\right)\left[\left(1-\frac{b_f}{b}\right)^2+3\left(1-\frac{c_f}{c}\right)^2\right]\right\}+\left(1-\frac{b_f}{b}\right)\left[3\left(1-2\frac{c_f}{c}\right)+\left(1-\frac{b_f}{b}\right)^2\right]\cos^{-1}\frac{1}{m}\sqrt{\frac{1-m^2\left(1-\frac{b_f}{b}\right)^2}{1-\left(1-\frac{b_f}{b}\right)^2}}+\left[3\left(1-\frac{c_f}{c}\right)\left(1-\frac{b_f}{b}\right)^2+\left(1-3\frac{c_f}{c}\right)\right]\cos^{-1}\left(1-\frac{b_f}{b}\right)\sqrt{\frac{m^2-1}{1-\left(1-\frac{b_f}{b}\right)^2}}\right)\right]$	$\frac{c_f}{c};\ \frac{c_f}{c}>\frac{m-1}{m}$ $\frac{m-1}{m};\ \frac{c_f}{c}<\frac{m-1}{m}$	$\frac{m-1}{m}+\frac{1}{m}\frac{c_f}{c}$

C_{h_α}	14	$C_{h_\alpha}=-\frac{2}{\beta}\frac{2}{\pi\beta\left[3\frac{b_f}{b}\left(\frac{c_f}{c}\right)^2-2\left(\frac{c_f}{c}\right)^3\right]}\left(\left(3\frac{c_f}{c}-1\right)\cos^{-1}\left[m\left(1-\frac{b_f}{b}\right)\right]+\left(1-\frac{c_f}{c}\right)^3\cos^{-1}\frac{m\left(1-\frac{b_f}{b}\right)}{1-\frac{c_f}{c}}-\right.$ $m\left(1-\frac{b_f}{b}\right)^3\left[\cosh^{-1}\frac{1}{m\left(1-\frac{b_f}{b}\right)}-\cosh^{-1}\frac{1-\frac{c_f}{c}}{m\left(1-\frac{b_f}{b}\right)}\right]+\frac{m}{\sqrt{m^2-1}}\left\{\frac{\pi}{2}\left(\frac{c_f}{c}\right)^2\left(3-\frac{c_f}{c}\right)+\left(1-\frac{b_f}{b}\right)\left[3\left(1-2\frac{c_f}{c}\right)+\right.\right.$ $\left.\left(1-\frac{b_f}{b}\right)^2\right]\cos^{-1}\frac{1}{m}\sqrt{\frac{1-m^2\left(1-\frac{b_f}{b}\right)^2}{1-\left(1-\frac{b_f}{b}\right)^2}}+\left[3\left(1-\frac{c_f}{c}\right)\left(1-\frac{b_f}{b}\right)^2+\left(1-3\frac{c_f}{c}\right)\right]\cos^{-1}\left(1-\frac{b_f}{b}\right)\sqrt{\frac{m^2-1}{1-\left(1-\frac{b_f}{b}\right)^2}}-$ $\left(1-\frac{b_f}{b}\right)\left[3\left(1-\frac{c_f}{c}\right)^2+\left(1-\frac{b_f}{b}\right)^2\right]\cos^{-1}\frac{1}{m}\sqrt{\frac{\left(1-\frac{c_f}{c}\right)^2-m^2\left(1-\frac{b_f}{b}\right)^2}{\left(1-\frac{c_f}{c}\right)^2-\left(1-\frac{b_f}{b}\right)^2}}-$ $\left.\left(1-\frac{c_f}{c}\right)\left[3\left(1-\frac{b_f}{b}\right)^2+\left(1-\frac{c_f}{c}\right)^2\right]\cos^{-1}\left(1-\frac{b_f}{b}\right)\sqrt{\frac{m^2-1}{\left(1-\frac{c_f}{c}\right)^2-\left(1-\frac{b_f}{b}\right)^2}}\right\}\right)$	$\frac{m-1}{m}+\frac{1}{m}\frac{c_f}{c}$	1.0

TABLE III.—CHARACTERISTICS OF INBOARD FLAPS ON TRIANGULAR WINGS

[$m<1$ or $m>1$; Mach lines ahead or behind leading edge]

Quantity	Equation number	Equation	Range		
			$(b_f/b)_{min}$	$(b_f/b)_{max}$	m
C_{L_δ}	15	$C_{L_\delta}=\frac{4}{\beta}\left(2\,\frac{b_f}{b}\,\frac{c_f}{c}\right)$	0	$1-\frac{1}{m}\,\frac{c_f}{c}$	<1
			0	$1-\frac{c_f}{c}$	>1
C_{l_δ}	16	$C_{l_\delta}=\frac{1}{\beta}\left[2\left(\frac{b_f}{b}\right)^2\frac{c_f}{c}\right]$	0	$1-\frac{1}{m}\,\frac{c_f}{c}$	<1
			0	$1-\frac{c_f}{c}$	>1
$C_{m_{C_L}}$	17	$C_{m_{C_L}}=-\frac{1}{4}\left(2-3\,\frac{c_f}{c}\right)$	0	$1-\frac{1}{m}\,\frac{c_f}{c}$	<1
			0	$1-\frac{c_f}{c}$	>1
C_{h_δ}	18	$C_{h_\delta}=-\frac{2}{\beta}\left(1-\frac{2c_f/c}{3m\pi b_f/b}\right)$	$\frac{1}{2m}\,\frac{c_f}{c}$	$1-\frac{m+1}{2m}\,\frac{c_f}{c}$	<1
			$\frac{1}{2m}\,\frac{c_f}{c}$	$1-\frac{c_f}{c}$	>1
C_{h_δ}	19	$C_{h_\delta}=-\frac{2}{\beta}\left[\frac{2}{\pi}\sin^{-1}\frac{2mb_f/b}{c_f/c}+\frac{2\left(\frac{c_f}{c}\right)^2+4m^2\left(\frac{b_f}{b}\right)^2}{3m\pi\,\frac{b_f}{b}\left(\frac{c_f}{c}\right)^2}\sqrt{\left(\frac{c_f}{c}\right)^2-4m^2\left(\frac{b_f}{b}\right)^2}-\frac{2c_f/c}{3m\pi b_f/b}\right]$	0	$1-\frac{m+1}{2m}\,\frac{c_f}{c};\ \frac{c_f}{c}>\frac{2m}{m+2}$ $\frac{1}{2m}\,\frac{c_f}{c};\ \frac{c_f}{c}<\frac{2m}{m+2}$	<1
			0	$1-\frac{c_f}{c};\ \frac{c_f}{c}>\frac{2m}{1+2m}$ $\frac{1}{2m}\,\frac{c_f}{c};\ \frac{c_f}{c}<\frac{2m}{1+2m}$	>1
C_{h_α}	20	$C_{h_\alpha}=-\frac{2}{\beta}\left[\frac{m}{\sqrt{m^2-1}}+\left(1-\frac{m}{\sqrt{m^2-1}}\right)\left(\frac{1-\frac{1}{3}\,\frac{c_f}{c}}{b_f/b}\right)\right]$	$1/m$	$1-\frac{c_f}{c}$	>1
C_{h_α}	21	$C_{h_\alpha}=-\frac{2}{\beta}\,\frac{2}{3\pi\,\frac{b_f}{b}\left(\frac{c_f}{c}\right)^2}\left[\frac{\pi}{2}\left(1-\frac{c_f}{c}\right)^3-\left(1-3\,\frac{c_f}{c}\right)\sin^{-1}\left(m\,\frac{b_f}{b}\right)+m\left(\frac{b_f}{b}\right)^3\cosh^{-1}\frac{1}{mb_f/b}-\right.$ $\frac{m}{\sqrt{m^2-1}}\left(\left[\left(\frac{b_f}{b}\right)^3+3\,\frac{b_f}{b}\left(1-2\,\frac{c_f}{c}\right)\right]\cos^{-1}\frac{1}{m}\sqrt{\frac{1-m^2\left(\frac{b_f}{b}\right)^2}{1-\left(\frac{b_f}{b}\right)^2}}+\left[3\left(\frac{b_f}{b}\right)^2\left(1-\frac{c_f}{c}\right)+\right.\right.$ $\left.\left.\left.\left(1-3\,\frac{c_f}{c}\right)\right]\cos^{-1}\frac{b_f}{b}\sqrt{\frac{m^2-1}{1-\left(\frac{b_f}{b}\right)^2}}-\frac{\pi}{2}\left\{\frac{b_f}{b}\left[3\left(1-\frac{c_f}{c}\right)^2+\left(\frac{b_f}{b}\right)^2\right]-\left(\frac{c_f}{c}\right)^2\left(3-\frac{c_f}{c}\right)\right\}\right)\right]$	$\frac{1}{m}\left(1-\frac{c_f}{c}\right)$	$1-\frac{c_f}{c};\ \frac{c_f}{c}>\frac{m-1}{m}$ $\frac{1}{m};\ \frac{c_f}{c}<\frac{m-1}{m}$	>1

C_{h_α}	22	$C_{h_\alpha}=-\frac{2}{\beta}\frac{2}{3\pi\frac{b_f}{b}\left(\frac{c_f}{c}\right)^2}\left(\left(1-\frac{c_f}{c}\right)^3\sin^{-1}\frac{mb_f/b}{1-\frac{c_f}{c}}-\left(1-3\frac{c_f}{c}\right)\sin^{-1}\left(m\frac{b_f}{b}\right)+m\left(\frac{b_f}{b}\right)^3\left(\cosh^{-1}\frac{1}{mb_f/b}-\cosh^{-1}\frac{1-\frac{c_f}{c}}{mb_f/b}\right)+\right.$ $\frac{m}{\sqrt{m^2-1}}\left\{\left[\left(\frac{b_f}{b}\right)^3+3\frac{b_f}{b}\left(1-\frac{c_f}{c}\right)^2\right]\cos^{-1}\frac{1}{m}\sqrt{\frac{\left(1-\frac{c_f}{c}\right)^2-m^2\left(\frac{b_f}{b}\right)^2}{\left(1-\frac{c_f}{c}\right)^2-\left(\frac{b_f}{b}\right)^2}}-\left[\left(\frac{b_f}{b}\right)^3-\right.\right.$ $\left.3\frac{b_f}{b}\left(1-2\frac{c_f}{c}\right)\right]\cos^{-1}\frac{1}{m}\sqrt{\frac{1-m^2\left(\frac{b_f}{b}\right)^2}{1-\left(\frac{b_f}{b}\right)^2}}+\left[3\left(\frac{b_f}{b}\right)^2\left(1-\frac{c_f}{c}\right)+\left(1-\frac{c_f}{c}\right)^3\right]\cos^{-1}\frac{b_f}{b}\sqrt{\frac{m^2-1}{\left(1-\frac{c_f}{c}\right)^2-\left(\frac{b_f}{b}\right)^2}}-$ $\left.\left.\left[3\left(\frac{b_f}{b}\right)^2\left(1-\frac{c_f}{c}\right)+\left(1-3\frac{c_f}{c}\right)\right]\cos^{-1}\sqrt{\frac{m^2-1}{1-\left(\frac{b_f}{b}\right)^2}}-\frac{\pi}{2}\left[3\left(\frac{c_f}{c}\right)^2-\left(\frac{c_f}{c}\right)^3\right]\right\}\right)$	0	$\frac{1}{m}\left(1-\frac{c_f}{c}\right)$	>1
C_{h_α}	23	$C_{h_\alpha}=-\frac{2}{\beta}\frac{m}{E(\sqrt{1-m^2})}\frac{1}{3\frac{b_f}{b}\left(\frac{c_f}{c}\right)^2}\left[\left(1-\frac{c_f}{c}\right)^3\sin^{-1}\frac{b_f/b}{1-\frac{c_f}{c}}-\left(1-3\frac{c_f}{c}\right)\sin^{-1}\frac{b_f}{b}-\frac{b_f}{b}\left(2-3\frac{c_f}{c}\right)\sqrt{1-\left(\frac{b_f}{b}\right)^2}+\right.$ $\left.2\frac{b_f}{b}\left(1-\frac{c_f}{c}\right)\sqrt{\left(1-\frac{c_f}{c}\right)^2-\left(\frac{b_f}{b}\right)^2}+\left(\frac{b_f}{b}\right)^3\left(\cosh^{-1}\frac{1}{b_f/b}-\cosh^{-1}\frac{1-\frac{c_f}{c}}{b_f/b}\right)\right]$	0	$1-\frac{c_f}{c}$	<1

TABLE IV.—CHARACTERISTICS OF FULL-TRIANGULAR-TIP FLAPS ON TRIANGULAR WINGS

[$m>1$, Mach lines behind leading edge]

Quantity	Equation number	Equation	Range	
			$(b_f/b)_{min}$	$(b_f/b)_{max}$
C_{L_δ}	24	$C_{L_\delta}=\frac{8}{\beta}\left(\frac{c_f}{c}\right)^2$	0	1.0
C_{l_δ}	25	$C_{l_\delta}=\frac{4}{\beta}\left(\frac{c_f}{c}\right)^2\left(1-\frac{c_f}{c}\right)$	0	1.0
$C_{m_{C_L}}$	26	$C_{m_{C_L}}=-\frac{1}{2}\left(1-\frac{c_f}{c}\right)$	0	1.0
C_{h_δ}	27	$C_{h_\delta}=-\frac{2}{\beta}$	0	1.0
C_{h_α}	28	$C_{h_\alpha}=-\frac{2}{\beta}\frac{m}{\sqrt{m^2-1}}$	0	$\frac{m-1}{m}$
C_{h_α}	29	$C_{h_\alpha}=-\frac{2}{\beta}\frac{m}{\sqrt{m^2-1}}+\frac{6m}{\pi\beta\left(\frac{c_f}{c}\right)^3\sqrt{m^2-1}}\left\{\left[-\frac{7}{12}+\frac{3}{2}\frac{c_f}{c}-\left(\frac{c_f}{c}\right)^2+\frac{1}{3}\left(\frac{c_f}{c}\right)^3\right]\pi-\frac{m^2-1+2m^2\left(1-\frac{c_f}{c}\right)^2}{6m^2\sqrt{m^2-1}}\sqrt{1-m^2\left(1-2\frac{c_f}{c}\right)^2}+\right.$ $\left(\frac{2}{3}-\frac{c_f}{c}\right)\frac{\sqrt{m^2-1}}{m}\cos^{-1}\left(m-2m\frac{c_f}{c}\right)-\frac{1}{3}\tan^{-1}\sqrt{\frac{m+1}{m-1}}+\frac{4m^2\left(1-\frac{c_f}{c}\right)^3}{3(m^2-1)}\tan^{-1}\sqrt{\frac{(m-1)\left[2m\frac{c_f}{c}-(m-1)\right]}{(m+1)\left[-2m\frac{c_f}{c}+(m+1)\right]}}+$ $\frac{7-25\frac{c_f}{c}+30\left(\frac{c_f}{c}\right)^2-12\left(\frac{c_f}{c}\right)^3}{6\left(1-\frac{c_f}{c}\right)}\sin^{-1}\sqrt{\frac{1-m^2\left(1-2\frac{c_f}{c}\right)^2}{m^2-m^2\left(1-2\frac{c_f}{c}\right)^2}}+\frac{9-18\frac{c_f}{c}+12\left(\frac{c_f}{c}\right)^2-4\left(\frac{c_f}{c}\right)^3}{6}$ $\left.\tan^{-1}\frac{2\left(1-\frac{c_f}{c}\right)-\sqrt{1-m^2\left(1-2\frac{c_f}{c}\right)^2}}{\left(1-2\frac{c_f}{c}\right)\sqrt{m^2-1}}+\frac{7-18\frac{c_f}{c}+12\left(\frac{c_f}{c}\right)^2-4\left(\frac{c_f}{c}\right)^3}{6}\tan^{-1}\frac{2\frac{c_f}{c}-\sqrt{1-m^2\left(1-2\frac{c_f}{c}\right)^2}}{\left(1-2\frac{c_f}{c}\right)\sqrt{m^2-1}}\right\}$	$\frac{m-1}{m}$	1.0

U. S. GOVERNMENT PRINTING OFFICE: 1950

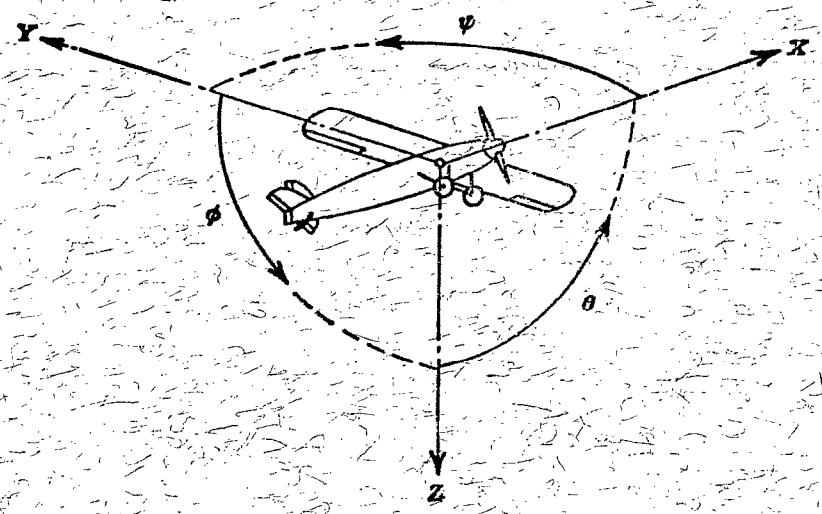

Positive directions of axes and angles (forces and moments) are shown by arrows

Axis		Force (parallel to axis) symbol	Moment about axis			Angle		Velocities	
Designation	Symbol		Designation	Symbol	Positive direction	Designation	Symbol	Linear (component along axis)	Angular
Longitudinal	X	X	Rolling	L	$Y \longrightarrow Z$	Roll	ϕ	u	p
Lateral	Y	Y	Pitching	M	$Z \longrightarrow X$	Pitch	θ	v	q
Normal	Z	Z	Yawing	N	$X \longrightarrow Y$	Yaw	ψ	w	r

Absolute coefficients of moment

$C_l=\frac{L}{qbS}$ (rolling) $\quad C_m=\frac{M}{qcS}$ (pitching) $\quad C_n=\frac{N}{qbS}$ (yawing)

Angle of set of control surface (relative to neutral position), δ. (Indicate surface by proper subscript.)

4. PROPELLER SYMBOLS

D Diameter

p Geometric pitch

p/D Pitch ratio

V' Inflow velocity

V_s Slipstream velocity

T Thrust, absolute coefficient $C_T=\frac{T}{\rho n^2 D^4}$

Q Torque, absolute coefficient $C_Q=\frac{Q}{\rho n^2 D^5}$

P Power, absolute coefficient $C_P=\frac{P}{\rho n^3 D^5}$

C_s Speed-power coefficient $=\sqrt[5]{\frac{\rho V^5}{P n^2}}$

η Efficiency

n Revolutions per second, rps

Φ Effective helix angle $=\tan^{-1}\left(\frac{V}{2\pi r n}\right)$

5. NUMERICAL RELATIONS

1 hp=76.04 kg-m/s=550 ft-lb/sec
1 metric horsepower=0.9863 hp
1 mph=0.4470 mps
1 mps=2.2369 mph

1 lb=0.4536 kg
1 kg=2.2046 lb
1 mi=1,609.35 m=5,280 ft
1 m=3.2808 ft